

# Conditional Spectral Analysis of Replicated Multiple Time Series with Application to Nocturnal Physiology

Robert T. Krafty, Ori Rosen, David S. Stoffer,  
Daniel J. Buysse, and Martica H. Hall \*

July 17, 2022

---

\*R. T. Krafty is Visiting Associate Professor, Department of Biostatistics, University of Pittsburgh (rkrafty@pitt.edu) and Assistant Professor, Department of Statistics, Temple University (krafty@temple.edu). O. Rosen is Professor, Department of Mathematical Science, University of Texas El Paso (ori@math.utep.edu). D. S. Stoffer is Professor, Department of Statistics (stoffer@pitt.edu), and D. J. Buysse and M. H. Hall are Professors, Department of Psychiatry, (buyssedj@upmc.edu, hallmh@upmc.edu), University of Pittsburgh. This work was supported by NIH grants R01GM113243, P01AG020677, R01HL104607, G12MD007592 and RR024153, NSF grants DMS1506882, 2G12MD007592 and DMS1512188, and NSA grant H98230-12-1-0246.

# Abstract

This article considers the problem of analyzing associations between power spectra of multiple time series and cross-sectional outcomes when data are observed from multiple subjects. The motivating application comes from sleep medicine, where researchers are able to non-invasively record physiological time series signals during sleep. The frequency patterns of these signals, which can be quantified through the power spectrum, contain interpretable information about biological processes. An important problem in sleep research is drawing connections between power spectra of time series signals and clinical characteristics; these connections are key to understanding biological pathways through which sleep affects, and can be treated to improve, health. Such analyses are challenging as they must overcome the complicated structure of a power spectrum from multiple time series as a complex positive-definite matrix-valued function. This article proposes a new approach to such analyses based on a tensor-product spline model of Cholesky components of outcome-dependent power spectra. The approach flexibly models power spectra as nonparametric functions of frequency and outcome while preserving geometric constraints. A Whittle likelihood based Markov chain Monte Carlo (MCMC) algorithm is developed for automated model fitting and for providing inference on associations between outcomes and any spectral measure. The method is used to analyze data from a study of sleep in older adults and uncovers new insights into how stress and arousal are connected to the amount of time one spends in bed.

KEY WORDS: Coherence; Heart Rate Variability; MCMC; Multivariate Time Series; Sleep; Smoothing Spline; Spectral Analysis; Tensor-Product ANOVA; Whittle Likelihood.

## 1 Introduction

Innovations in data collection and storage have led to an increase in the number of biomedical studies that record multiple time series signals and outcome measures in multiple subjects. For many time series, including common signals such as blood pressure, heart rate and electrochromatography (EEG), frequency patterns that are quantied through the power

spectrum contain important information about biological processes. Consequently, studies whose goals are to understand how underlying biological mechanisms are connected to behavioral and clinical outcomes often require an analysis of associations between outcomes and power spectra of multiple time series.

Our motivating application comes from a sleep study whose goal is to better understand the pathways that connect sleep to health and functioning. In the study, heart rate variability (HRV) is recorded in subjects during a night of sleep. HRV is measured through the series of elapsed times between consecutive heart beats, and its power spectrum provides indirect measures of psychological stress and physiological arousal (Hall et al., 2007). Upon awakening, subjects reported subjectively assessed sleep outcomes, such as the amount of time slept during the night, which are associated with many aspects of well-being (Buysse, 2014). Understanding the association between the power spectrum of HRV during different sleep periods (i.e. beginning, middle and end of the night) and self-reported sleep outcomes is essential to understanding how stress connects sleep to health and, consequently, for guiding the use of treatments of poor sleep.

In the biomedical literature, a two-stage approach is typically used to analyze such data. In the first stage, power collapsed within preselected frequency bands is estimated individually for each time series (Malik et al., 1996; Hall et al., 2004). A power spectrum is a function of frequency; power collapsed within a frequency band is an integral of the power spectrum over a range of frequencies, which converts the functional parameter into a scalar measure. In the second stage, classical statistical methods, such as ANOVA and linear regression, are used to evaluate associations between these band-collapsed spectral measures and outcomes. Such an approach has three major drawbacks. First, it is highly dependent on the frequency-band collapsed measures selected and there exists a hot debate as to which measures should be considered and/or how they should be interpreted (Burr, 2007). Ideally, an analysis of such data should provide global measures that can be used to understand the entire system while also providing a means to conduct inference on any frequency band-collapsed measure of potential interest. Second, estimated power is treated as if it were not an estimate but the

true unknown parameter, leading to inaccurate inference. Finally, band-specific frequency measures are estimated for each time series separately, inhibiting the evaluation of patterns across series. For instance, in our motivating example, this two-stage approach is unable to examine how the coherence in HRV between the beginning and end of the night is connected to sleep outcomes.

In the statistics literature, a considerable amount of research has been conducted on methods for analyzing functional variables that utilize the entire functional data. Reviews of some of these developments are given by Ramsay and Silverman (2005) and Wang et al. (2016). Included in this body of work are methods for analyzing associations between power spectra and outcomes when one time series is observed per subject (Fokianos and Savvides, 2008; Stoffer et al., 2010; Krafty and Hall, 2013). The power spectrum is a positive function and, to preserve this positivity, the logarithm of spectra are modeled. When one observes multiple time series per subject and interest lies in frequency patterns both within each series and across different series, the problem becomes considerably more challenging. This is the case in our motivating study where we are interested not only in stress and arousal during particular periods of sleep, but also in their persistence and coherence across periods. While the power spectrum from a single time series is a positive real-valued function of frequency, the power spectrum from multiple time series is a positive-definite Hermitian matrix valued function of frequency. An analysis of associations between power spectra from multiple time series and study outcomes must be able to flexibly model associations while preserving this positive-definite Hermitian structure.

Efficient nonparametric methods that preserve the positive-definite Hermitian structure of spectral matrices have been developed for the simpler, classical problem of estimating the power spectrum of a multivariate time series from a single subject by modeling Cholesky components of spectral matrices as functions of frequency (Dai and Guo, 2004; Rosen and Stoffer, 2007; Krafty and Collinge, 2013). In this article, we extend this framework to develop a new approach to analyzing data from multiple subjects that models Cholesky components as functions of both frequency and outcome. Rather than being curves as functions of

frequency, components of spectral matrices under the proposed model are surfaces. Changes in these surfaces with respect to the outcome provide nonparametric measures of association between outcomes and power spectra. An MCMC algorithm based on the Whittle likelihood, or the asymptotic likelihood derived from the Fourier transform of the data, is developed for model fitting and inference. The method allows one to evaluate the entire outcome-dependent power spectrum and to conduct nonparametric inference on the association between the outcome and any function of the power spectrum.

The rest of the article is organized as follows. Our motivating application, the AgeWise Sleep Study, is discussed in Section 2. A review of spectral analysis in the classical setting, where data are observed from a single subject, is given in Section 3. The proposed methodology for analyzing time series from multiple subjects is presented in Section 4: the conditional power spectrum is defined in Section 4.1, the tensor-product ANOVA model is presented in Section 4.2, and the Whittle likelihood and smoothing priors are discussed in Section 4.3. The proposed method is used to analyze data from the motivating application in Section 5 and some final remarks are offered in Section 6.

## 2 The AgeWise Sleep Study

An estimated 43% of older adults report problems initiating or maintaining sleep (Foley et al., 1995). Poor sleep in older adults has been linked to depression, heart disease, obesity, arthritis, diabetes, lung disease and stroke (Foley et al., 2004). With medical and scientific advances leading to an increase in the world’s elderly population, the consequences of poor sleep in older adults pose a major public health concern. The AgeWise study is a NIH-funded Program Project conducted at the University of Pittsburgh that seeks a better understanding of causes, effects, and treatments of poor sleep in older adults. Towards this goal, we consider  $N = 108$  men and women between 69–89 years of age who were observed during a night of in-home sleep as part of the AgeWise Study. Two types of data were collected in each subject. First, subjects were observed during the night through ambulatory polysomnography (PSG), or the continuous collection of electrophysiological changes that occur during sleep. Second,

upon awakening, subjects completed the Pittsburgh Sleep Diary (Monk et al., 1994) to record self-reported sleep outcomes during the night.

As previously discussed, HRV is the series of elapsed times between heart beats. It is of interest to researchers, as it reflects neurological control of the heart, and through this capacity, its power spectrum provides indirect measures of stress reactivity and arousal. The PSG used in the study included an electrocardiograph (ECG) to monitor heart activity. The ECG was used to locate the timing of heart beats, which were then differenced, detrended, cubic spline interpolated, and resampled at 1 Hz to compute HRV series throughout the night.

During the night, the body cycles through two types of sleep: rapid eye movement (REM) and non-rapid eye movement (NREM) sleep. In NREM sleep, which contains deep-sleep, the parasympathetic branch of the autonomic nervous system that is responsible for unconscious actions and stimulates the body to “rest-and-digest” dominates the sympathetic branch, which drives the “flight-or-fight” response. Parasympathetic nervous system activity during NREM is hypothesized to be responsible for many of the rejuvenating properties of sleep (Siegel, 2005). Physiological activity during NREM sleep is not constant; in good sleepers, the amount of parasympathetic activity during NREM increases throughout the night (Hall et al., 2004). To enable an analysis that can evaluate autonomic nervous system activity and its changes during the night, we consider 3 HRV time series per subject (at the beginning, middle, and end of the night) by extracting the first 5 minutes of HRV from the first three periods of NREM sleep. Data from two subjects are displayed in Figure 1.

The goal of our analysis is to understand how the power spectrum of HRV over the three periods of NREM are connected to self-reported sleep. We focus on one particular self-reported sleep measure derived from the Pittsburgh Sleep Diary: time in bed (TIB). TIB is defined as the elapsed time between attempted sleep and final wakening. It serves as an upper bound for the amount of time spent asleep during the night, which has been linked to heart disease, hypertension, impaired neurobehavioral performance and mortality (Buysse, 2014). The reported TIB from our sample has a mean of 477.99 minutes and a

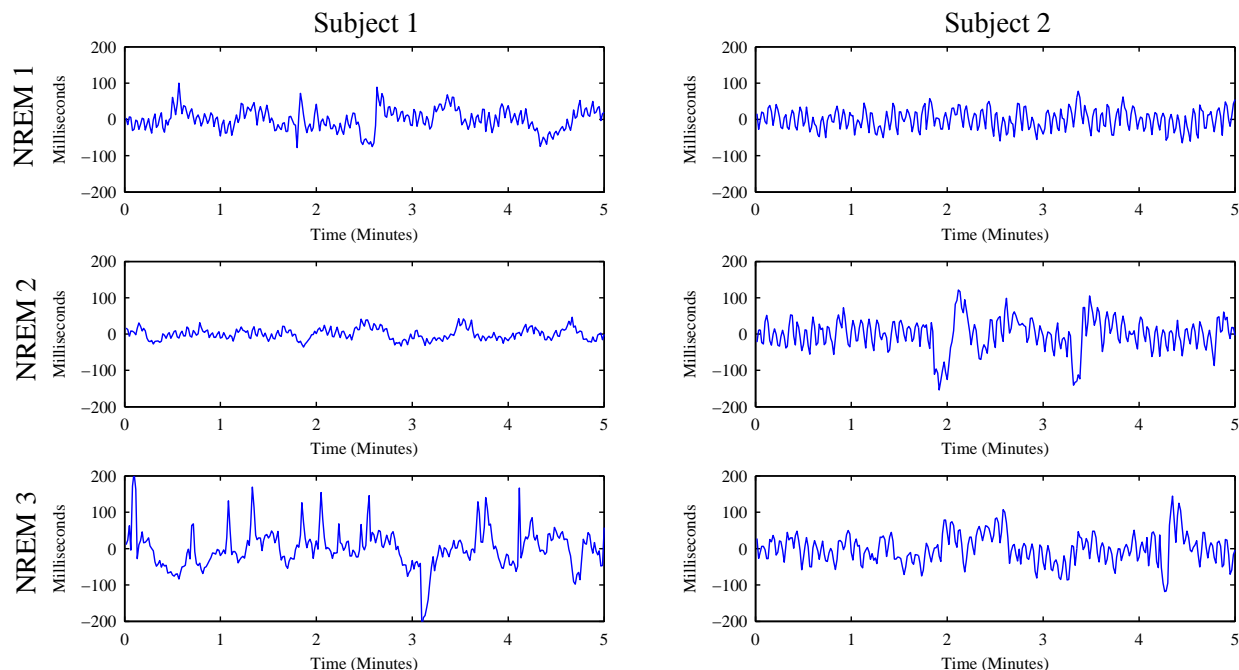


Figure 1: Detrended HRV time series during the first three periods of NREM from two subjects. Subject 1 reported a TIB of 357.67 minutes and subject 2 reported a TIB of 521.00 minutes.

standard deviation of 71.32 minutes. The resulting data for analysis consist of three epochs of HRV, one during each of the first three periods of NREM sleep, and self-reported TIB from each subject.

### 3 Methodological Background: Spectral Domain Analysis

Before introducing our proposed model for the spectral analysis of multiple time series from multiple subjects in Section 4, in this section we present background on spectral analysis in the classical setting, where data are observed from a single subject, for both univariate and multivariate time series.

## 3.1 Univariate Time Series

### 3.1.1 Population Parameters

Spectral domain analysis focuses on the cyclic behavior of time series data. An alternate approach is time domain analysis wherein the relationship between the data at different time lags is the focus. For stationary time series, the main time domain tool is the covariance between a current value of the series, say  $X_t$ , and the value of the series  $h$  time units prior, say  $X_{t-h}$ . The autocovariance is a function of lag, and is given by

$$\gamma(h) = \text{Cov}(X_t, X_{t-h}), \quad h = 0, \pm 1, \pm 2, \dots$$

If  $\gamma(h)$  is absolutely summable (which it is for ARMA models, for example), then there is a duality between the power spectrum, given by

$$f(\omega) = \sum_{h=-\infty}^{\infty} \gamma(h) \exp(-2\pi i \omega h), \quad \omega \in \mathbb{R},$$

and the autocovariance function, namely,

$$\gamma(h) = \int_{-1/2}^{1/2} f(\omega) \exp(2\pi i \omega h) d\omega, \quad h = 0, \pm 1, \pm 2, \dots, \quad (1)$$

as the inverse transform of the power spectrum. The relationship is the same as that of a characteristic function and a probability density. Consequently, the information contained in the power spectrum is equivalent to the information contained in the autocovariance function. If we are concerned with lagged behavior, working with  $\gamma(h)$  is more informative; if we are concerned with cyclic behavior, as is the case of HRV where cyclical behavior provides interpretable physiological information, working with  $f(\omega)$  is more informative.

The fact that, when the time series is purely stochastic,  $\gamma(h)$  is positive definite, ensures  $f(\omega) > 0$  for all  $\omega$ . In addition to being positive,  $f$  has two other restrictions as a function of frequency. By the nature of the Fourier transform, it is periodic such that  $f(\omega) = f(\omega + 1)$ , and it is a Hermitian function, or an even function, where  $f(\omega) = f(-\omega)$ . Consequently,  $f(\omega)$  is usually displayed only for  $\omega \in [0, 1/2]$ .



Putting  $h = 0$  in (1) yields

$$\gamma(0) = \text{Var}(X_t) = \int_{-1/2}^{1/2} f(\omega) d\omega,$$

which expresses the total variance of the time series as the integrated power spectrum. In particular, we may think of  $f(\omega) d\omega$  as the approximate variance in the data attributed to frequencies in a small band of width  $d\omega$  around  $\omega$ . For example, average monthly temperatures contain a strong component of one cycle every year (hot in the summer, cold in the winter). The power spectrum of such data will have a large relative peak at the frequency  $\omega = \frac{1 \text{ cycle}}{12 \text{ months}}$ . We can interpret this result by saying that most of the variability in the data can be attributed to the annual cycle. It is common to view spectral analysis as an analysis of variance (ANOVA) of time series data with respect to frequency. In fact, the power spectrum is a density of variance rather than of probability.

### 3.1.2 Estimation

The nonparametric estimation of  $f$  from an epoch of length  $n$ ,  $X_1, \dots, X_n$ , can begin by considering the discrete Fourier transformation (DFT)

$$Y_m = n^{-1/2} \sum_{t=1}^n X_t \exp(-2\pi i \omega_m t),$$

where  $\omega_m = m/n$  are the Fourier frequencies. When  $n$  is large,  $Y_m$  are approximately independent mean-zero complex normal random variables with variances  $f(\omega_m)$  for  $m = 1, \dots, \lfloor n/2 \rfloor$ ,  $\lfloor n/2 \rfloor$  is the integer part of  $n/2$ , and  $Y_m = Y_{m+1/2}$  (Shumway and Stoffer, 2011, Appendix C). Consequently, the periodogram  $|Y_m|^2$  provides approximately unbiased but noisy estimates of  $f(\omega_m)$ . Consistent estimates can be obtained by smoothing the periodogram across frequency using tools such as local averaging (Shumway and Stoffer, 2011, Chapter 4.5), splines (Wahba, 1980; Pawitan and O'Sullivan, 1994; Qin and Wang, 2008), and wavelets (Moulin, 1994).

Our estimation approach for multiple time series from multiple subjects, which we discuss in Section 4, is based on Bayesian smoothing splines. For illustration purposes, we present the

univariate approach here. The spline approach balances the fit of an estimator to observed data with a roughness based measure of regularity. There are many different formulations of splines (Wood, 2006); we consider the Bayesian formulation that was first discussed by Kimeldorf and Wahba (1970). In this formulation, when regularization is based on second derivatives, or cubic splines are used, a function is decomposed into linear and nonlinear parts. Nonlinear parts are modeled through a basis reflecting smoothness, regularization is achieved through smoothing priors on the nonlinear parts, and the likelihood function provides a measure of fit to the data. The large sample distribution of  $Y_m$  provides the Whittle likelihood (Whittle, 1953, 1954)

$$L(Y | f) \approx \prod_{m=1}^M f^{-1}(\omega_m) \exp\{-f^{-1}(\omega_m) |Y_m|^2\}, \quad (2)$$

where  $M = \lfloor (n - 1)/2 \rfloor$ . We adopt generic notation throughout this article where  $Y$  will denote all DFT data. Since we assume  $f$  is a positive function, to facilitate unrestricted optimization, we model  $\log f$  rather than  $f$  itself. The linear part of a periodic even function is a constant. A basis for the non-linear part that reflects the periodic and even structure is

$$J(\omega_i, \omega_j) = -[\kappa_4(|\omega_i - \omega_j|) + \kappa_4(\omega_i + \omega_j - \lfloor \omega_i + \omega_j \rfloor)]/2, \quad (3)$$

where  $\kappa_1(\omega) = \omega - .5$ ,  $\kappa_2(\omega) = [\kappa_1^2(\omega) - 1/12]/2$  and  $\kappa_4(\omega) = [\kappa_1^4(\omega) - \kappa_1^2(\omega)/2 + 7/240]/24$  are the scaled Bernoulli polynomials (Krafty and Collinge, 2013). The model is thus

$$\log f(\omega) = a + \sum_{m=1}^M c_m J(\omega, \omega_m). \quad (4)$$

Regularization is achieved by assuming the prior  $(c_1, \dots, c_M)^T \sim N(\mathbf{0}, \tau^2 J^{-1})$  where  $J = \{J(\omega_i, \omega_j)\}$  is the  $M \times M$  matrix evaluated at the Fourier frequencies. The smoothing parameter  $\tau^2 > 0$  balances the smoothness of the Bayes estimator to its fit to the data, where the estimate approaches a constant as  $\tau^2 \rightarrow 0$  and where it interpolates  $|Y_m|^2$  as  $\tau^2 \rightarrow \infty$ . Inference can either be done conditional on  $\tau^2$ , or a prior distribution could be placed on  $\tau^2$  for unconditional inference.

The equivalence between penalized likelihood and Bayes estimation (Kimeldorf and Wahba, 1970) implies that the Bayes estimator under this model for a fixed  $\tau^2$  is equivalent to the

frequentist estimator that minimizes a penalized Whittle likelihood (Pawitan and O’Sullivan, 1994; Qin and Wang, 2008). It should be noted that, to avoid the complications discussed in Section 2 of Krafty and Collinge (2013) and facilitate Bayesian computation, our model is presented under a slightly different formulation from Pawitan and O’Sullivan (1994) and Qin and Wang (2008), who consider a Whittle likelihood over all frequencies  $\omega_m$ ,  $m = 1, \dots, n$ , and model  $\log f$  as periodic, but not as an even function.

## 3.2 Multivariate Time Series

### 3.2.1 Population Parameters

The ideas presented in Section 3.1 generalize to the multivariate case wherein we observe a  $P$ -dimensional vector-valued time series, say  $\{\mathbf{X}_t\}$ . Under stationarity, the autocovariance function is a  $P \times P$  matrix given by

$$\Gamma(h) = \text{Cov}(\mathbf{X}_t, \mathbf{X}_{t-h}), \quad h = 0, \pm 1, \pm 2, \dots$$

If  $\sum_h \|\Gamma(h)\| < \infty$ , the spectral density matrix of the series  $\mathbf{X}_t$  is given by

$$f(\omega) = \sum_{h=-\infty}^{\infty} \Gamma(h) \exp(-2\pi i \omega h), \quad \omega \in \mathbb{R}$$

and the inverse relationship is

$$\Gamma(h) = \int_{-1/2}^{1/2} f(\omega) \exp(2\pi i \omega h) d\omega, \quad h = 0, \pm 1, \pm 2, \dots$$

For each  $\omega \in \mathbb{R}$ ,  $f(\omega)$  is a  $P \times P$  non-negative definite Hermitian matrix with the diagonal elements,  $f_{pp}(\omega)$  for  $p = 1, \dots, P$ , being the spectra of the individual components, and the off-diagonal elements,  $f_{qp}(\omega)$  for  $q \neq p = 1, \dots, P$ , being the cross-spectra. Throughout this article, we assume that  $f(\omega)$  is non-singular for all  $\omega \in \mathbb{R}$ . As in the univariate case,  $f$  is a periodic and Hermitian function of frequency. For matrix-valued functions, Hermitian as a function of frequency is defined as  $f(\omega) = f^*(-\omega)$ , where  $f^*(\omega)$  is the complex conjugate of  $f(\omega)$ . Equivalently, real components are even functions,  $\Re\{f_{pq}(\omega)\} = \Re\{f_{pq}(-\omega)\}$ , and imaginary components are odd functions,  $\Im\{f_{pq}(\omega)\} = -\Im\{f_{pq}(-\omega)\}$ .

An important example of the application of the cross-spectrum is to the problem of linearly predicting one of the component series, say  $X_{qt}$ , from another component, say  $X_{pt}$ . A measure of the strength of such a relationship is the squared coherence function defined as

$$\rho_{qp}^2(\omega) = \frac{|f_{qp}(\omega)|^2}{f_{qq}(\omega)f_{pp}(\omega)}.$$

This is analogous to conventional squared correlation between two finite-variance random variables; e.g.,  $0 \leq \rho_{qp}^2(\omega) \leq 1$ . This analogy motivates the interpretation of squared coherence as the squared correlation between two time series at frequency  $\omega$ . These ideas extend in an obvious way to the concept of multiple coherence and partial coherence functions obtained from the full spectral matrix in much the same way that multiple correlation and partial correlation can be obtained from a covariance matrix. Full details of these results may be found in Shumway and Stoffer (2011, Chapters 4 & 7)

### 3.2.2 Estimation

In the multivariate setting, let

$$\mathbf{Y}_m = n^{-1/2} \sum_{t=1}^n \mathbf{X}_t \exp(-2\pi i \omega_m t)$$

be the DFTs of the data. In this case, the Whittle likelihood is

$$L(Y | f) \approx \prod_{m=1}^M |f^{-1}(\omega_m)| \exp\{-\mathbf{Y}_m^* f^{-1}(\omega_m) \mathbf{Y}_m\},$$

and, as in the univariate setting, the periodogram  $\mathbf{Y}_m \mathbf{Y}_m^*$  is an approximately unbiased but noisy estimate of  $f(\omega_m)$  from which consistent estimates can be obtained by smoothing.

While, in the univariate setting, the spectrum is smoothed on the logarithmic scale to preserve positivity, Cholesky components of spectral matrices can be smoothed to preserve positive-definiteness in the multivariate setting (Dai and Guo, 2004; Rosen and Stoffer, 2007; Krafty and Collinge, 2013). The modified Cholesky decomposition assures that, for a spectral matrix  $f(\omega)$ , there exists a unique  $P \times P$  lower triangular complex matrix  $\Theta(\omega)$  with ones

on the diagonal and a unique  $P \times P$  positive diagonal matrix  $\Psi(\omega)$  such that

$$f^{-1}(\omega) = \Theta(\omega)\Psi^{-1}(\omega)\Theta^*(\omega).$$

There are  $P^2$  Cholesky components to estimate:  $\Re\{\Theta_{k\ell}(\omega)\}$  and  $\Im\{\Theta_{k\ell}(\omega)\}$  for  $k > \ell = 1, \dots, P-1$ , and  $\Psi_{kk}^{-1}(\omega)$  for  $k = 1, \dots, P$ . Since the diagonal terms  $\Psi_{kk}(\omega) > 0$ , we model  $\log \Psi_{kk}^{-1}$ . The real components are periodic even functions and we model them in the same manner as (4)

$$\begin{aligned} \Re\{\Theta_{k\ell}(\omega)\} &= a_{rk\ell} + \sum_{m=1}^M c_{rk\ell m} J(\omega, \omega_m), \quad k > \ell = 1, \dots, P-1 \\ \log \Psi_{kk}^{-1}(\omega) &= a_{dkk} + \sum_{m=1}^M c_{dkk m} J(\omega, \omega_m), \quad k = 1, \dots, P, \end{aligned}$$

where  $r$  and  $d$  are used to denote coefficients for real components of  $\Theta$  and the logarithm of diagonal components of  $\Psi$ , respectively ( $i$  will be used for imaginary components), and we assume the priors  $(c_{rk\ell 1}, \dots, c_{rk\ell M})^T \sim N(\mathbf{0}, \tau_{rk\ell}^2 J^{-1})$  and  $(c_{dkk 1}, \dots, c_{dkk M})^T \sim N(\mathbf{0}, \tau_{dkk}^2 J^{-1})$ . Imaginary components are odd functions, so that  $\Im\{\Theta_{k\ell}(0)\} = 0$  and, consequently, their linear components are null. Nonlinear components that reflect periodic and odd restrictions can be modeled using

$$K(\omega_i, \omega_j) = \{\kappa_4(\omega_i + \omega_j - \lfloor \omega_i + \omega_j \rfloor) - \kappa_4(|\omega_i - \omega_j|)\} / 2, \quad (5)$$

so that

$$\Im\{\Theta_{k\ell}(\omega)\} = \sum_{m=1}^M c_{ik\ell m} K(\omega, \omega_m), \quad k > \ell = 1, \dots, P-1.$$

Regularization is achieved through the prior  $(c_{ik\ell 1}, \dots, c_{ik\ell M})^T \sim N(\mathbf{0}, \tau_{ik\ell}^2 K^{-1})$ , where  $K = \{K(\omega_i, \omega_j)\}$  is the  $M \times M$  matrix at the Fourier frequencies (Krafty and Collinge, 2013).

## 4 Methodology: Replicated Multiple Time Series

### 4.1 Conditional Power Spectrum

The primary question considered in this article is how to assess the association between the power spectrum of  $P$ -variate time series of length  $n$ ,  $\{\mathbf{X}_{j1}, \dots, \mathbf{X}_{jn}\}$ , and a real-valued

variable  $U_j$  from  $j = 1, \dots, N$  independent subjects. In the motivating study, there are  $N = 108$  participants,  $U_j$  is self-reported TIB, and  $\mathbf{X}_{jt}$  are time series of HRV during the first  $P = 3$  periods of NREM. Without loss of generality, the methodology is presented under the assumption that the variable  $U_j$  is scaled to be in the interval  $[0,1]$ .

To assess this relationship, we define the conditional power spectrum

$$f(\omega, u) = \sum_{\tau=-\infty}^{\infty} \text{Cov}(\mathbf{X}_{jt}, \mathbf{X}_{j,t+\tau} \mid U_j = u) e^{-2\pi i \omega \tau}, \quad \omega \in \mathbb{R}, u \in [0, 1].$$

As with the power spectrum of a single multivariate time series, the spectral matrices  $f(\omega, u)$  are positive-definite  $P \times P$  Hermitian matrices, and  $f(\cdot, u)$  is a periodic and Hermitian function of frequency for fixed  $u$ . In a traditional spectral analysis without a cross-sectional variable, spectral measures such as  $f_{pq}$  and  $\rho_{pq}^2 = |f_{pq}|^2 / (f_{pp}f_{qq})$  are curves as functions of frequency. In the conditional setting, these are surfaces as functions of both frequency and the variable  $u$ . How these functions change with respect to  $u$  provides information as to how spectral measures are associated with the variable.

## 4.2 Tensor-Product ANOVA Model

To flexibly model the conditional power spectrum as a function of both  $\omega$  and  $u$  while preserving the positive-definite and Hermitian constraints, we use tensor product ANOVA models on the  $P^2$  unique components of the modified Cholesky decomposition

$$f^{-1}(\omega, u) = \Theta(\omega, u)\Psi^{-1}(\omega, u)\Theta^*(\omega, u),$$

$\Re\{\Theta_{k\ell}(\omega, u)\}$ ,  $\Im\{\Theta_{k\ell}(\omega, u)\}$  for  $k > \ell = 1, \dots, P - 1$ , and  $\log \Psi_{kk}^{-1}(\omega, u)$  for  $k = 1, \dots, P$ .

We first present the tensor-product model given basis functions, and then describe how the basis functions are obtained. Let  $u_j$ ,  $j = 1, \dots, N$ , be the observed values of the outcome variable,  $Q_H$  be the matrix of basis functions for nonlinear functions of  $u$  evaluated at the observed data,  $Q_J$  be the matrix of basis functions for nonlinear real functions of  $\omega$ ,  $Q_K$  be the matrix of basis functions for nonlinear imaginary functions of  $\omega$ ,  $Q_L$  be the matrix of basis functions of linear functions of  $u$ , and  $\mathbf{1}_M$  be the  $M$ -vector of ones that will model

linear real functions of  $\omega$ . To write the tensor-product model, concatenate components across frequency and outcome to define

$$\boldsymbol{\theta}_{kl} = [\{\Theta_{k\ell}(\omega_1, u_1), \dots, \Theta_{k\ell}(\omega_M, u_1)\}, \dots, \{\Theta_{k\ell}(\omega_1, u_N), \dots, \Theta_{k\ell}(\omega_M, u_N)\}]'$$

for  $k > \ell = 1, \dots, P-1$  and similarly define  $\log \boldsymbol{\psi}_{kk}^{-1}$  for  $k = 1, \dots, P$ . The real and imaginary parts of  $\boldsymbol{\theta}_{kl}$ , and  $\log \boldsymbol{\psi}_{kk}^{-1}$  can then be expressed as

$$\begin{aligned} \Re\{\boldsymbol{\theta}_{kl}\} &= \{Q_L \otimes \mathbf{1}_M\} \mathbf{a}_{rkl} + \{Q_H \otimes \mathbf{1}_M\} \mathbf{b}_{rkl} + \{Q_L \otimes Q_J\} \mathbf{c}_{rkl} + \{Q_H \otimes Q_J\} \mathbf{d}_{rkl} \\ \Im\{\boldsymbol{\theta}_{kl}\} &= \{Q_L \otimes Q_K\} \mathbf{c}_{ikl} + \{Q_H \otimes Q_K\} \mathbf{d}_{ikl} \\ \log \boldsymbol{\psi}_{kk}^{-1} &= \{Q_L \otimes \mathbf{1}_M\} \mathbf{a}_{dkk} + \{Q_H \otimes \mathbf{1}_M\} \mathbf{b}_{dkk} + \{Q_L \otimes Q_J\} \mathbf{c}_{dkk} + \{Q_H \otimes Q_J\} \mathbf{d}_{dkk}, \end{aligned}$$

where the  $r$ ,  $i$  and  $d$  subscripts on the coefficient vectors  $\mathbf{a}$ ,  $\mathbf{b}$ ,  $\mathbf{c}$  and  $\mathbf{d}$  stand for real, imaginary and diagonal, respectively. In this tensor-product model,  $\mathbf{a}$  are coefficients for functions that are linear in both  $\omega$  and  $u$ ,  $\mathbf{b}$  are coefficients for functions that are linear in  $\omega$  and nonlinear in  $u$ ,  $\mathbf{c}$  are coefficients for functions that are nonlinear in  $\omega$  and linear in  $u$ , and  $\mathbf{d}$  are coefficients for functions that are nonlinear in both  $\omega$  and  $u$ . Note that, since the periodic odd restrictions of imaginary functions of frequency imply that linear terms are null, coefficients  $\mathbf{a}$  and  $\mathbf{b}$  are not present in the model of  $\Im\{\boldsymbol{\theta}_{kl}\}$ .

Recall the  $M \times M$  matrices  $J$  and  $K$  defined by evaluating the functions in (3) and (5) at the Fourier frequencies. The scaled eigenvectors of these matrices are used as bases to model nonlinear components of  $\omega$  and provide a scalable MCMC algorithm based on diagonal covariance priors for model fitting in Section 4.3. Define the spectral decomposition  $J = V_J D_J V_J'$  from which  $Q_J = V_J D_J^{1/2}$ . The matrix  $Q_K$  is similarly obtained. For functions of the outcome  $u$ , note that these functions have no restrictions. Consequently, we model linear parts using  $Q_L = \{(1 \quad u_i)'\}$  and nonlinear parts using  $Q_H = V_H D_H^{1/2}$  where  $H = V_H D_H V_H'$  is the spectral decomposition of the  $N \times N$  matrix  $H = \{H(u_i, u_j)\}$  and

$$H(u_i, u_j) = \kappa_2(u_i)\kappa_2(u_j) - \kappa_4(|u_i - u_j|)$$

is a standard reproducing kernel for unrestricted cubic smoothing splines (Gu, 2013). Note that for smoothing splines, the number of columns of  $Q_H$ ,  $Q_J$  and  $Q_K$  are in principle  $N$ ,  $M$ , and  $M$ , respectively. However the eigenvalues associated with the columns decay geometrically and, in practice, much smaller values can be taken without affecting fit, resulting

in substantial computational saving. In our application, we use 10 basis functions for each of these matrices, but for simplicity we do not introduce further notation.

### 4.3 The Likelihood, Priors and Sampling Scheme

#### The Likelihood

The DFT for the  $j$ th subject at frequency  $\omega_m$  is given by

$$\mathbf{Y}_{jm} = n^{-1/2} \sum_{t=1}^n \mathbf{X}_{jt} \exp(-2\pi i \omega_m t)$$

and, for large  $n$ , its large sample distribution conditional on  $u_j$  leads to the conditional Whittle likelihood

$$L(Y | f) \approx \prod_{j=1}^N \prod_{m=1}^M |f^{-1}(\omega_m, u_j)| \exp\{-\mathbf{Y}_{jm}^* f^{-1}(\omega_m, u_j) \mathbf{Y}_{jm}\}.$$

#### Priors

We define smoothing priors to regularize the fitted components based on integrated squared second derivatives. Let  $Q_r = \begin{pmatrix} Q_L \otimes \mathbf{1}_M & \vdots & Q_H \otimes \mathbf{1}_M & \vdots & Q_L \otimes Q_J & \vdots & Q_H \otimes Q_J \end{pmatrix}$  and  $\boldsymbol{\eta}_{rkl} = (\mathbf{a}'_{rkl}, \mathbf{b}'_{rkl}, \mathbf{c}'_{rkl}, \mathbf{d}'_{rkl})'$ , then  $\mathfrak{R}\{\boldsymbol{\theta}_{kl}(\omega, u)\} = Q_r \boldsymbol{\eta}_{rkl}$ . Denoting  $\boldsymbol{\eta}_{dkk} = (\mathbf{a}'_{dkk}, \mathbf{b}'_{dkk}, \mathbf{c}'_{dkk}, \mathbf{d}'_{dkk})'$  and setting  $Q_d = Q_r$ ,  $\log \boldsymbol{\psi}_{kk}^{-1} = Q_d \boldsymbol{\eta}_{dkk}$ . To model  $\mathfrak{S}\{\boldsymbol{\theta}_{kl}(\omega, u)\}$ , let  $Q_i = \begin{pmatrix} Q_L \otimes Q_K & \vdots & Q_H \otimes Q_K \end{pmatrix}$  and  $\boldsymbol{\eta}_{ikl} = (\mathbf{c}'_{ikl}, \mathbf{d}'_{ikl})'$ , then  $\mathfrak{S}\{\boldsymbol{\theta}_{kl}(\omega, u)\} = Q_i \boldsymbol{\eta}_{ikl}$ .

The priors are now specified as follows.

1.  $\boldsymbol{\eta}_{rkl} \stackrel{\text{ind}}{\sim} N(\mathbf{0}, D_{rkl})$ , where  $D_{rkl} = \text{diag}(\sigma_\alpha^2 \mathbf{1}'_{n_a}, \tau_{\beta rkl}^2 \mathbf{1}'_{n_b}, \tau_{\gamma rkl}^2 \mathbf{1}'_{n_c}, \tau_{\delta rkl}^2 \mathbf{1}'_{n_d})$ ,  $k > \ell = 1, \dots, P-1$ , and  $\mathbf{1}_{n_a}, \mathbf{1}_{n_b}, \mathbf{1}_{n_c}$  and  $\mathbf{1}_{n_d}$  are unit vectors of lengths  $n_a = 2$ ,  $n_b = N$ ,  $n_c = 2M$  and  $n_d = MN$ , respectively. The variance  $\sigma_\alpha^2$  is fixed at a large value.
2.  $\boldsymbol{\eta}_{ikl} \stackrel{\text{ind}}{\sim} N(\mathbf{0}, D_{ikl})$ , where  $D_{ikl} = \text{diag}(\tau_{\gamma ikl}^2 \mathbf{1}'_{n_c}, \tau_{\delta ikl}^2 \mathbf{1}'_{n_d})$ ,  $k > \ell = 1, \dots, P-1$ .
3.  $\boldsymbol{\eta}_{dkk} \stackrel{\text{ind}}{\sim} N(\mathbf{0}, D_{dkk})$ , where  $D_{dkk} = \text{diag}(\sigma_\alpha^2 \mathbf{1}'_{n_a}, \tau_{\beta dkk}^2 \mathbf{1}'_{n_b}, \tau_{\gamma dkk}^2 \mathbf{1}'_{n_c}, \tau_{\delta dkk}^2 \mathbf{1}'_{n_d})$ ,  $k = 1, \dots, P$ .



4. The priors on  $\tau_{\beta r k \ell}^2$ ,  $\tau_{\gamma r k \ell}^2$ ,  $\tau_{\delta r k \ell}^2$ ,  $\tau_{\gamma i k \ell}^2$ ,  $\tau_{\delta i k \ell}^2$ ,  $k > \ell = 1, \dots, P - 1$ ,  $\tau_{\beta d k k}^2$ ,  $\tau_{\gamma d k k}^2$ ,  $\tau_{\delta d k k}^2$ ,  $k = 1, \dots, P$ , are independent Half- $t(\nu, G)$  (Gelman, 2006) with pdf  $p(x) \propto [1 + (x/G)^2/\nu]^{-(\nu+1)/2}$ ,  $x > 0$ , where the hyperparameters  $\nu$  and  $G$  are assumed known. The larger the value of  $G$ , the less informative the prior. In our computations,  $G = 10$  and  $G = 10^5$  gave indistinguishable results. Computationally, it is convenient to utilize the following scale mixture representation (Wand et al., 2012):  $(\tau^2 | g) \sim IG(\nu/2, \nu/g)$ ,  $g \sim IG(1/2, 1/G^2)$ , where  $IG(a, b)$ , is the inverse Gamma distribution with pdf  $p(x) \propto x^{-(a+1)} \exp(-b/x)$ ,  $x > 0$ .

## Sampling Scheme

1. The basis function coefficient vectors  $\boldsymbol{\eta}_{r k \ell}$  and  $\boldsymbol{\eta}_{i k \ell}$  are drawn from multivariate normal distributions.
2. The basis function coefficient vectors  $\boldsymbol{\eta}_{d k k}$  are drawn in a Metropolis-Hastings step from their conditional posterior distribution

$$\log p(\boldsymbol{\eta}_{d k k} | Q_d, \mathbf{v}_k, D_{d k k}) \stackrel{c}{=} \sum_{j=1}^N \sum_{m=1}^M \left\{ \mathbf{q}'_{d j m} \boldsymbol{\eta}_{d k k} - \exp(\mathbf{q}'_{d j m} \boldsymbol{\eta}_{d k k}) v_{k j m} \right\} - \frac{1}{2} \boldsymbol{\eta}'_{d k k} D_{d k k}^{-1} \boldsymbol{\eta}_{d k k},$$

where  $\mathbf{q}'_{d j m}$  is the row of  $Q_d$  corresponding to the  $j$ th subject and  $m$ th frequency,  $\mathbf{v}_k$  is a vector with components  $v_{k j m}$  depending on the DFTs and on other parameters held fixed, and  $\stackrel{c}{=}$  denotes equality up to a constant.

3. Each  $\tau^2$  is drawn from an inverse gamma distribution, conditional on another parameter.

Further details on the sampling scheme are given in Appendix B.

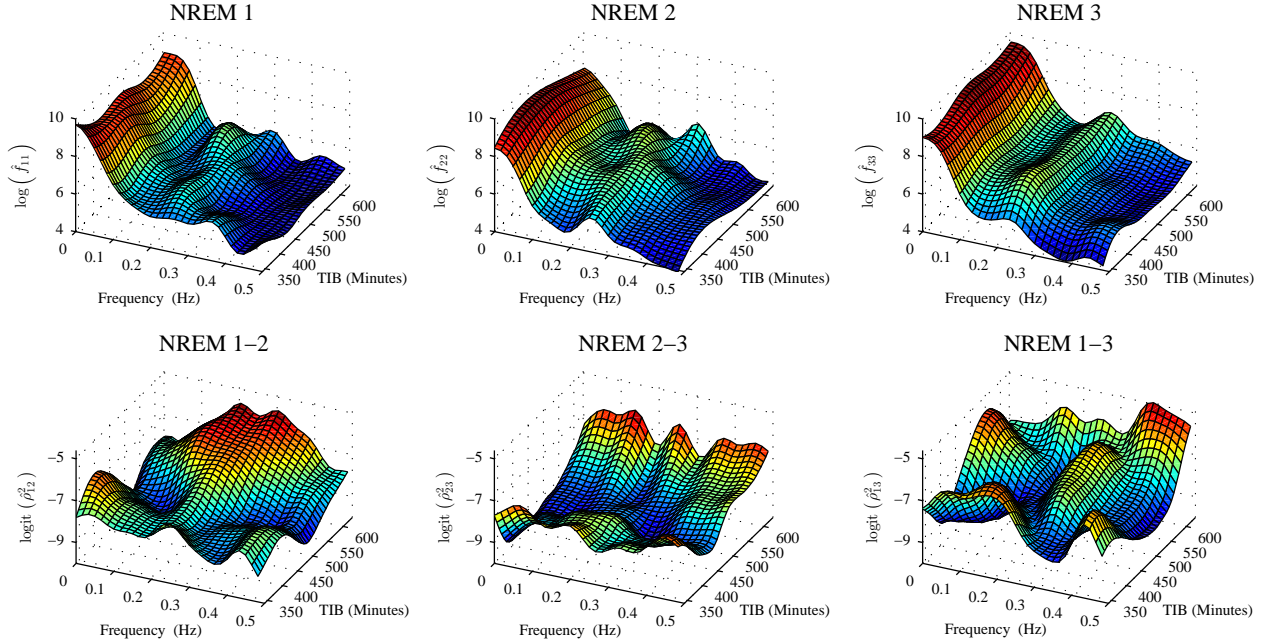


Figure 2: Estimated conditional log-spectra for each period of NREM (top panel) and estimated logit of conditional coherence between each period (bottom panel).

## 5 Application to the AgeWise Study

### 5.1 Analysis of the Conditional Spectrum

We used the proposed methodology to analyze the association between TIB and the power spectrum of the first three periods of NREM from  $N = 108$  AgeWise subjects, as described in Section 2. The results from this analysis provide new insights into biological underpinnings of spending too little or too much time in bed. In particular, our analysis suggests that (i) short TIB is connected to elevated stress and arousal within-periods of NREM towards the end of the night and (ii) long TIB is associated with a persistence in arousal in the beginning of the night.

Point estimates of the within-period conditional log-spectral surfaces,  $\log \{f_{pp}(\omega, u)\}$ , and of the cross-period conditional logit squared coherence surfaces,  $\text{logit} \{\rho_{pq}^2(\omega, u)\} = \log [\rho_{pq}^2(\omega, u) / \{1 - \rho_{pq}^2(\omega, u)\}]$  are displayed in Figure 2. These estimates are plotted on the logarithmic and logistic scales, respectively, to aid visualization. The conditional spectra at

each of the first three periods of NREM and the squared coherence between NREM 1 and 2 display different characteristics within low frequencies that are less than 0.15 Hz compared to higher frequencies between 0.15–0.40 Hz.

From a biological perspective, these results are not surprising and produce interpretable measures. As was discussed in Section 2, the autonomic nervous system is classically divided into two branches: the parasympathetic branch that is responsible for activities related to resting and digestion and the sympathetic branch that is responsible for the flight-or-fight response. Researchers have shown that power within the high frequency band (HF) within 0.15-0.40 Hz provides a measure of parasympathetic nervous system activity and that power within the low frequency band (LF) between 0.04-0.15 Hz is a measure of the combined modulation of both the sympathetic and parasympathetic nervous systems. Consequently, the ratio of power from low frequencies versus high frequencies (LF/HF) can be interpreted as a measure of sympathetic modulation relative to parasympathetic modulation. Blunted HF and elevated LF/HF power are often interpreted as indirect measures of physiological arousal and psychological stress (Hall et al., 2004, 2007). To obtain inference on associations between these measures and TIB, in the next two subsections we examine power and coherence collapsed within these bands as functions of TIB.

## 5.2 Analysis of Within-Period Power

We consider two collapsed measures of within-period power, HF and LF/HF, computed as

$$f_p^{HF}(u) = \int_{.15}^{.40} f_{pp}(\omega, u) d\omega$$

$$f_p^{LF/HF}(u) = \left\{ \int_{.04}^{.15} f_{pp}(\omega, u) d\omega \right\} / \left\{ \int_{.15}^{.40} f_{pp}(\omega, u) d\omega \right\}.$$

Estimates and 95% pointwise credible intervals for these two measures as functions of TIB are displayed in Figure 3 for each period.

HF power is relatively constant across TIB during NREM 1, while participants with a TIB of less than 400 minutes have decreased HF power during NREM 2 and 3 compared

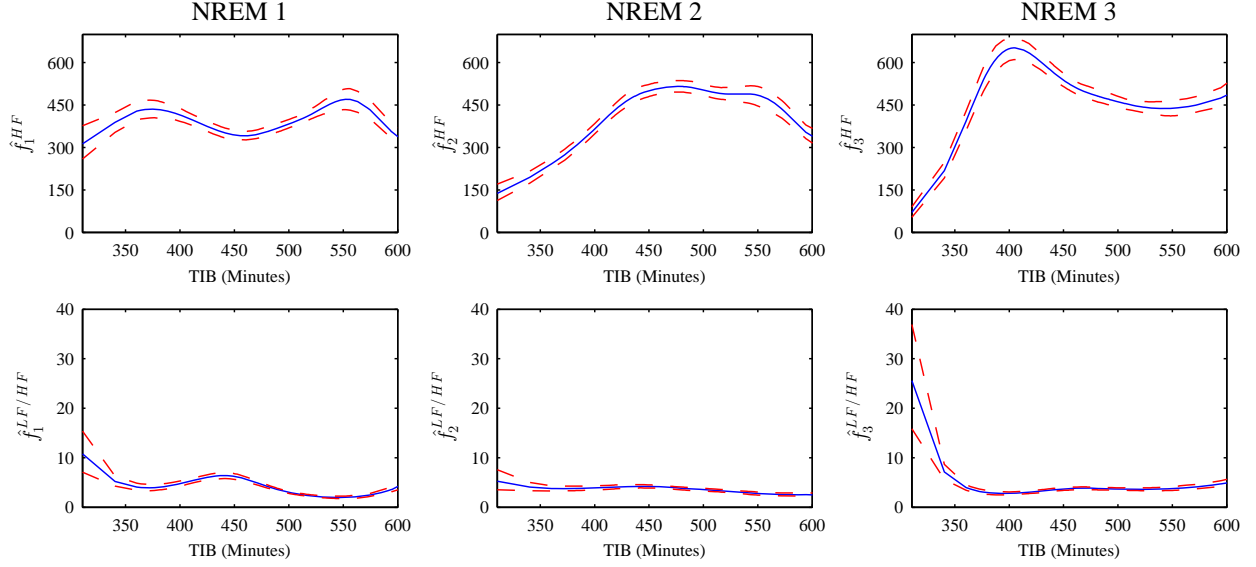


Figure 3: Estimated conditional HF (top panel),  $\hat{f}_p^{HF}$ , and LF/HF (bottom panel),  $\hat{f}_p^{LF/HF}$ , as functions of TIB with 95% pointwise credible intervals for each period of NREM.

to those who spend more time in bed. Further, those who have an exceedingly small TIB display increased LF/HF power during NREM sleep compared to those who spend more TIB during NREM 3. These characteristics are indicative of heightened physiological arousal and psychological stress.

Sleeping less than 7 hours per night has been shown to be associated with a multitude of negative health effects, including increased mortality (Buysse, 2014). The results of our analysis provide a potential pathway through which short sleep, which is inherently bounded by TIB, is connected to well-being: through increased stress and arousal towards the end of the night.

### 5.3 Analysis of Cross-Period Coherence

To investigate connections between cross-period coherence and TIB, we consider conditional HF band-squared coherence

$$\rho_{pq}^{2, HF}(u) = \left| \int_{.15}^{.40} f_{pq}(\omega, u) d\omega \right|^2 / \{f_p^{HF}(u) f_q^{HF}(u)\}$$

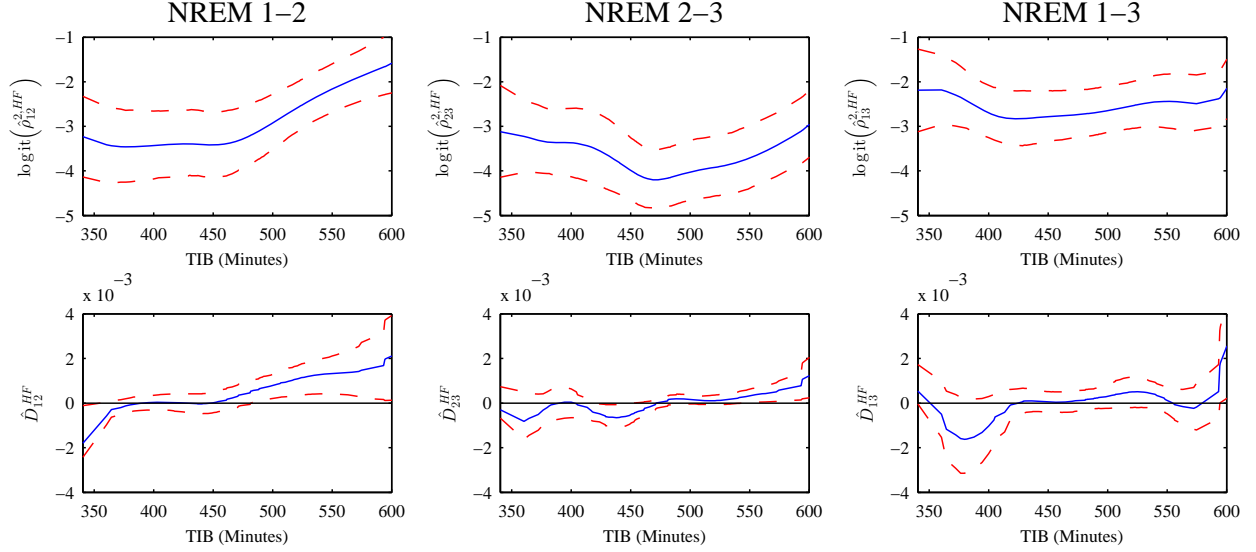


Figure 4: Estimated logit of integrated HF coherence (top panel),  $\text{logit}(\hat{\rho}_{pq}^{2,HF})$ , between each NREM period as functions of TIB and their first derivatives (bottom panel),  $\hat{D}_{pq}^{HF}$ , with pointwise 95% credible intervals.

and display estimates on the logit scale,  $\text{logit}(\rho_{pq}^{2,HF}) = \log[\rho_{pq}^{2,HF}/(1 - \rho_{pq}^{2,HF})]$ , in the top panel of Figure 4. To better understand how changes in TIB are associated with HF coherence, we also examine first derivatives,

$$D_{pq}^{HF}(u) = d[\rho_{pq}^{2,HF}(u)]/du,$$

whose estimates are displayed in the bottom panel of Figure 4. We find that the derivative of HF coherence between NREM 1 and 2 is positive for TIB greater than 500 minutes. This indicates that excessive increases in the amount of time spent in bed are associated with increased coherence in parasympathetic activity in the beginning of the night.

The relationship between excessive TIB and ill-health led Youngstedt and Kripke (2004) to propose modest sleep restrictions to increase quality of life and survival, especially for older adults, who tend to spend more time in bed as compared to younger adults. However, these restrictions must be used with great care as they can potentially lead to negative health effects (Reynolds III et al., 2010; Reynold et al., 2014). Our results demonstrate that excessive TIB is associated with a coherence in parasympathetic activity in the beginning of the night that is not present in moderate and short TIB. A possible explanation for this

relationship is that extensive TIB can cause an increase in the amount of time spent awake while in bed, or led to fragmented sleep. The roles of and relationships between physiological activity during different sleep cycles could change as sleep becomes more fragmented. These findings provide some of the first potential insights into the biological pathway through which excessive TIB can be connected to negative health, which can potentially be used to inform optimal sleep restriction strategies in older adults.

## 6 Final Remarks

This article introduces a novel approach to analyzing associations between multiple time series and cross-sectional outcomes when data are observed from multiple subjects. A new measure of association, the conditional power spectrum, is introduced and its Cholesky components are modeled as bivariate functions of frequency and cross-sectional outcome. An MCMC algorithm is developed for model fitting and allows for inference on any function of the power spectrum. The method was motivated by a sleep study and uncovered connections between excessive time in bed and heightened arousal and stress that could not have been uncovered through traditional methods.

We conclude this section by discussing three extensions to the proposed methodology. First, the model is formulated to investigate the association between power spectra and a single cross-sectional variable. The model could easily be extended through higher-order tensor product models to include multiple variables, such as the amount of time it takes to fall asleep and the number of awakenings during the night. However, such a model would provide inference on the effect of these variables on the power spectrum conditional on the other variables, complicating interpretation when these variables are highly correlated. Future work will explore an interpretable canonical correlation type dimension reduction of a collection of correlated variables and multivariate spectral matrices, which can be viewed as a multivariate extension of Krafty and Hall (2013). Second, our application focused on HRV, due to the insights that it provides into autonomic nervous system activity. One could also explore the spectral analysis of other PSG channels, as well as the simultaneous coupling

of channels. However, each channel of the PSG is sampled at a different rate. The second extension will develop conditional spectral analysis of time series with different sampling rates. Finally, since we were motivated by the analysis of HRV during epochs within NREM that are approximately stationary, we focused on stationary time series. For more highly sampled signals such as EEG, this assumption is not valid. A conditional time-frequency analysis for signals that are locally stationary will also be explored.

## Supplementary Material

**Appendices A and B:** Two supplementary appendices appear at the end of this manuscript.

Appendix A provides results from simulation studies and Appendix B contains details concerning the sampling scheme.

## References

- Burr, R. L. (2007), “Interpretation of normalized spectral heart rate variability indices in sleep research: A critical review,” *Sleep*, 30, 913–919.
- Buysse, D. J. (2014), “Sleep health: Can we define it? Does it matter?” *Sleep*, 37, 9–17.
- Dai, M. and Guo, W. (2004), “Multivariate spectral analysis using Cholesky decomposition,” *Biometrika*, 91, 629–643.
- Fokianos, K. and Savvides, A. (2008), “On comparing several spectral densities,” *Technometrics*, 50, 317–331.
- Foley, D. J., Ancoli-Israel, S., Britz, P., and Walsh, J. (2004), “Sleep disturbances and chronic disease in older adults: Results of the 2003 National Sleep Foundation Sleep in America Survey,” *Journal of Psychosomatic Research*, 56, 497–502.
- Foley, D. J., Monjan, A. A., Brown, S. L., Simonsick, E. M., Wallace, R. B., and Blazer, D. G. (1995), “Sleep complaints among elderly persons: An epidemiologic study of three communities.” *Sleep*, 18, 425–432.

- Gelman, A. (2006), “Prior distributions for variance parameters (Comment on article by Browne and Draper),” *Bayesian Analysis*, 1, 515–534.
- Gu, C. (2013), *Smoothing Spline ANOVA Models*, New York: Springer-Verlag, 2nd ed.
- Hall, M., Thayer, J., Germain, A., Moul, D., Vasko, R., Puhl, M., Miewald, J., and Buysse, D. (2007), “Psychological stress is associated with heightened physiological arousal during NREM sleep in primary insomnia,” *Behavioral Sleep Medicine*, 5, 178–193.
- Hall, M., Vasko, R., Buysse, D., Ombao, H., Chen, Q., Cashmere, J., Kupfer, D., and Thayer, J. (2004), “Acute stress affects heart rate variability during sleep,” *Psychosomatic Medicine*, 66, 56–62.
- Kimeldorf, G. S. and Wahba, G. (1970), “A correspondence between Bayesian estimation on stochastic processes and smoothing by splines,” *Annals of Mathematical Statistics*, 41, 495–502.
- Krafty, R. T. and Collinge, W. O. (2013), “Penalized multivariate Whittle likelihood for power spectrum estimation,” *Biometrika*, 100, 447–458.
- Krafty, R. T. and Hall, M. (2013), “Canonical correlation analysis between time series and static outcomes, with application to the spectral analysis of heart rate variability,” *Annals of Applied Statistics*, 7, 570–587.
- Loader, C. R. (1999), “Bandwidth selection: classical or plug-in?” *Annals of Statistics*, 27, 415–438.
- Malik, M., Bigger, J. T., Camm, A. J., Kleiger, R. E., Malliani, A., Moss, A. J., and Schwartz, P. J. (1996), “Heart rate variability - standards of measurement, physiological interpretation, and clinical use,” *Circulation*, 93, 1043–1065.
- Monk, T., Reynolds, C. F., Kupfer, D. J., Buysse, D. J., Coble, P. A., Hayes, A. J., MacHen, M. A., Petrie, S. R., and Ritenour, A. M. (1994), “The Pittsburgh Sleep Diary,” *Journal of Sleep Research*, 3, 111–120.



- Moulin, P. (1994), “Wavelet thresholding techniques for power spectrum estimation,” *IEEE Transactions on Signal Processing*, 42, 3126–3136.
- Pawitan, Y. and O’Sullivan, F. (1994), “Nonparametric spectral density estimation using penalized Whittle likelihood,” *Journal of the American Statistical Association*, 89, 600–610.
- Qin, L. and Wang, Y. (2008), “Nonparametric spectral analysis with applications to seizure characterization using EEG time series,” *Annals of Applied Statistics*, 2, 1432–1451.
- Ramsay, J. O. and Silverman, B. W. (2005), *Functional Data Analysis*, Springer Series in Statistics, Springer, 2nd ed.
- Reynold, A. M., Bowles, E. R., Saxena, A., Fayad, R., and Youngstedt, S. D. (2014), “Negative effects of time in bed extensions: A pilot study,” *Journal of Sleep Medicine and Disorders*, 1, 1002.
- Reynolds III, C. F., Serody, L., Okun, M. L., Hall, M. H., Houck, P. R., Patrick, S., Maurer, J., Bensasi, S., Mazumdar, S., Bell, B., Nebes, R. D., Miller, M. D., Dew, M. A., and Nofzinger, E. A. (2010), “Protecting sleep, promoting health in later life: A randomized clinical trial,” *Psychosomatic Medicine*, 72, 178–186.
- Rosen, O. and Stoffer, D. (2007), “Automatic estimation of multivariate spectra via smoothing splines,” *Biometrika*, 94, 335–345.
- Shumway, R. H. and Stoffer, D. S. (2011), *Time Series Analysis and Its Applications: With R Examples*, New York: Springer, 3rd ed.
- Siegel, J. M. (2005), “Clues to the functions of mammalian sleep,” *Nature*, 437, 1264–1271.
- Stoffer, D. S., Han, S., Qin, L., and Guo, W. (2010), “Smoothing spline ANOPOW,” *Journal of Statistical Planning and Inference*, 140, 3789–3796.
- Wahba, G. (1980), “Automatic smoothing of the log-periodogram,” *Journal of the American Statistical Association*, 75, 122–132.

- Wand, M., Ormerod, J., Padoan, S., and Frühworth, R. (2012), “Mean field variational Bayes for elaborate distributions,” *Bayesian Analysis*, 7, 847–900.
- Wang, J.-L., Chiou, J.-M., and Müller, H.-G. (2016), “Review of Functional Data Analysis,” *Annual Review of Statistics and Its Application*, 3, In Press.
- Whittle, P. (1953), “Estimation and information in stationary time series,” *Arkiv for Matematik*, 2, 423–434.
- (1954), “Some recent contributions to the theory of stationary processes,” *A Study in the Analysis of Stationary Time Series*, 2, 196–228.
- Wood, S. N. (2006), *Generalized Additive Models: An Introduction with R*, Boca Raton: CRC Press.
- Youngstedt, S. D. and Kripke, D. F. (2004), “Long sleep and mortality: Rationale for sleep restriction,” *Sleep Medicine Review*, 8, 159–174.

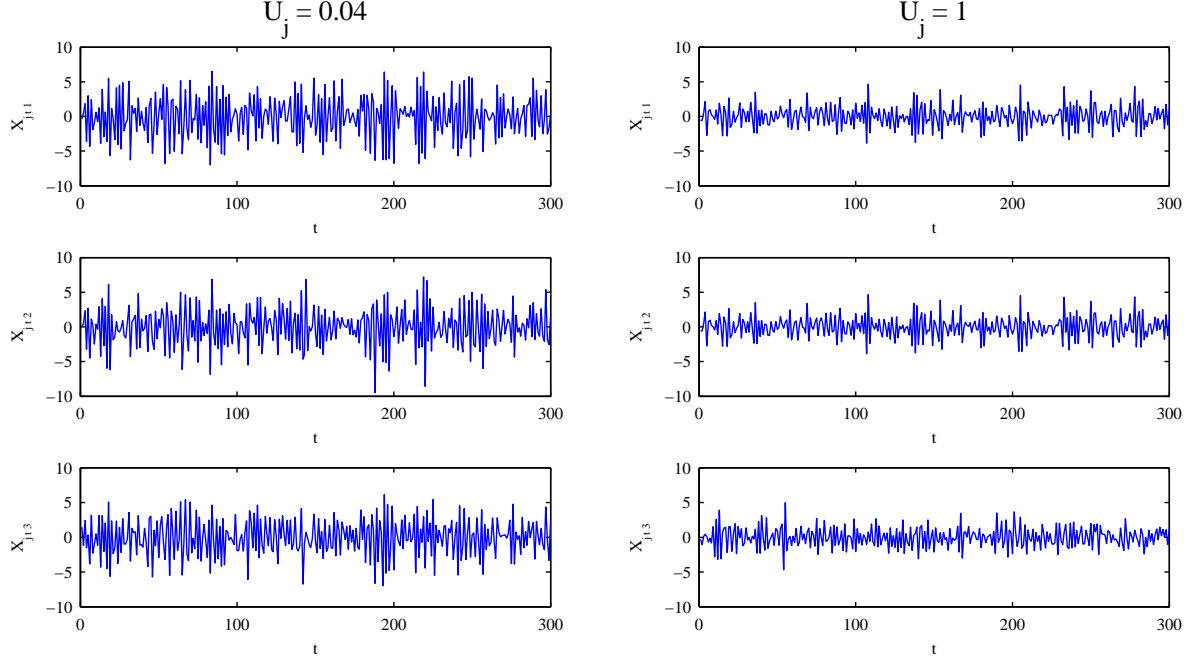


Figure A.1: Simulated conditional MA(2) epochs of length  $n = 300$  with  $u_j = 0.04$  and  $u_j = 1$ .

## A Simulation Study

To illustrate the proposed model and to investigate its empirical properties, we consider the  $P = 3$  dimensional second order moving average model ( MA(2) )

$$\mathbf{X}_{jt} = \boldsymbol{\epsilon}_{jt} + \Theta_1 \boldsymbol{\epsilon}_{jt-1} + \Theta_2 \boldsymbol{\epsilon}_{jt-2}, \quad j = 1, \dots, N, \quad t = 1, \dots, n,$$

where  $\Theta_1 = -I$ ,  $\Theta_2 = 0.6I$ ,  $I$  is the  $3 \times 3$  identity matrix, and  $\boldsymbol{\epsilon}_{jt}$  are independent  $N[\mathbf{0}, \Omega(u_j)]$  random variables with

$$\Omega(u) = \sigma^2(u) \begin{bmatrix} 1 & \rho(u) & \rho(u) \\ \rho(u) & 1 & \rho(u) \\ \rho(u) & \rho(u) & 1 \end{bmatrix},$$

$\sigma^2(u) = (2 - u)^2$  and  $\rho(u) = 0.6 - 0.25 \cos(\pi u)$ . Two simulated epochs of length  $n = 300$ , one with  $u_j = 0.04$  and one with  $u_j = 1$ , are displayed in Figure A.1. The conditional spectrum is given by

$$f(\omega, u) = \Theta(\omega) \Omega(u) \Theta(\omega)^*,$$

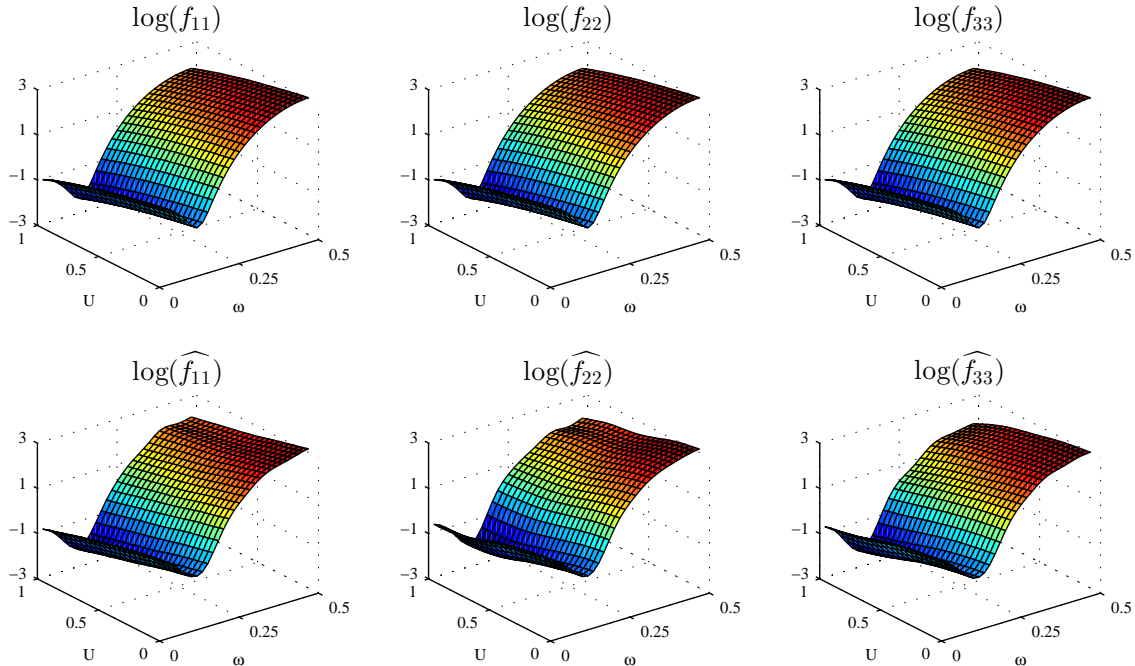


Figure A.2: Conditional log-spectra from the MA(2) model (top panels) and estimated conditional log-spectra from a random sample of time series of length  $n = 300$  from  $N = 25$  subjects (lower panels).

where  $\Theta(\omega) = I + \Theta_1 \exp(-2\pi i\omega) + \Theta_2 \exp(-4\pi i\omega)$ . The log-spectra,  $\log[f_{pp}(\omega, u)]$ , and their estimates under the proposed procedure from a random sample of  $N = 25$  independent epochs of length  $n = 300$  are displayed in Figure A.2. Plots of the logit-squared coherence,  $\text{logit}[\rho_{pq}^2(\omega, u)]$ , and their estimates are displayed in Figure A.3. The band-collapsed measures  $f_p^{HF}(u)$ ,  $f_p^{LF/HF}(u)$  and  $\rho_{pq}^{2,HF}(u)$ , along with their estimates and 95% credible intervals, are displayed in Figure A.4.

We simulated 100 random samples of conditional MA(2) time series of length  $n$  from  $N$  subjects with  $u_j = j/N$  for the four combinations of  $n = 300, 500$  and  $N = 25, 50$ . The estimation procedure was run using 10 bases for functions of  $\omega$ , 5 bases for functions of  $u$ , and for 2000 iterations of the MCMC algorithm with burn-in of 500 iterations. To investigate the sensitivity of the proposed estimation procedure with respect to hyperparameters, the procedure was run twice: for  $G = 10^5$  and for  $G = 10^{10}$ . To investigate the performance of the proposed procedure for conducting inference on band-collapsed measures as functions of

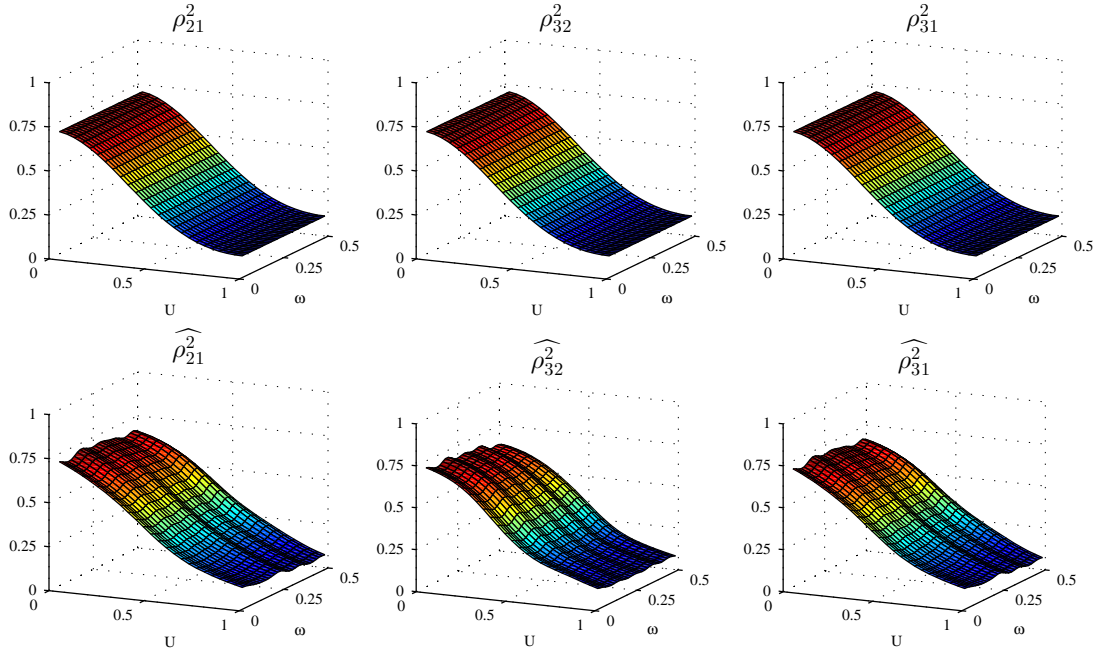


Figure A.3: Conditional squared coherence from the MA(2) model (top panels) and estimated conditional squared coherence from a random sample of time series of length  $n = 300$  from  $N = 25$  subjects (lower panels).

outcome, we computed pointwise 95% credible intervals for the nine band-collapsed curves  $f_1^{HF}$ ,  $f_2^{HF}$ ,  $f_3^{HF}$ ,  $f_1^{LF/HF}$ ,  $f_2^{LF/HF}$ ,  $f_3^{LF/HF}$ ,  $\rho_{12}^{2,HF}$ ,  $\rho_{23}^{2,HF}$ , and  $\rho_{13}^{2,HF}$ . The mean and standard deviation of pointwise coverage probabilities integrated across  $u$  are given in Table A.1. The integrated coverage was near the nominal 95% level for each component, ranging between 94.3%–97.4%. Coverage probabilities under different tuning parameters were indistinguishable.

To compare the performance of the proposed procedure to existing approaches, we also computed two two-stage estimators of within-period band-collapsed measures. In the first stage, periodograms were calculated and summed within HF and LF bands for each of the  $P = 3$  series for each of the  $N$  subjects to obtain raw subject-specific estimates. The raw subject-specific HF and LF/HF estimates were then smoothed across  $u$ . For the first estimator, smoothing was achieved by fitting a cubic smoothing spline with smoothing parameter selected through generalized cross-validation (GCV) (Gu, 2013). For the second estimator, smoothing was achieved through local linear regression with plug-in bandwidth (Loader,

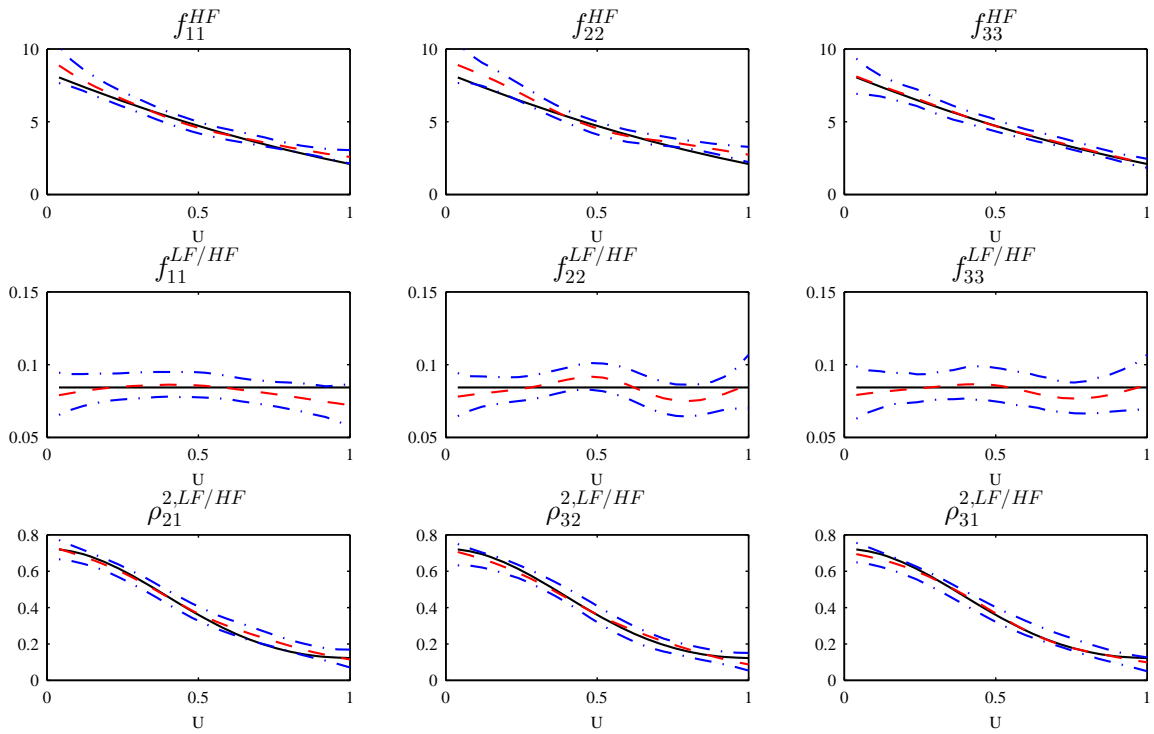


Figure A.4: HF band power (top panels), LF/HF band power (middle panels), and HF band squared coherence (bottom panel) (—), along with point estimates (---) and 95% credible intervals (- · -) from a random sample of  $N = 25$  conditional MA(2) time series of length  $n = 300$ .

$n$	$N$	$G$	$f_1^{HF}$	$f_2^{HF}$	$f_3^{HF}$	$f_1^{LF/HF}$	$f_2^{LF/HF}$	$f_3^{LF/HF}$	$\rho_{12}^{2,HF}$	$\rho_{23}^{2,HF}$	$\rho_{13}^{2,HF}$
300	25	$10^5$	.943 (.112)	.968 (.073)	.958 (.097)	.969 (.084)	.965 (.078)	.961 (.093)	.968 (.058)	.951 (.083)	.963 (.078)
		$10^{10}$	.943 (.112)	.968 (.073)	.958 (.097)	.969 (.084)	.965 (.078)	.961 (.093)	.968 (.058)	.951 (.083)	.963 (.078)
500	25	$10^5$	.968 (.070)	.949 (.087)	.969 (.070)	.965 (.097)	.974 (.062)	.967 (.069)	.968 (.068)	.950 (.086)	.963 (.083)
		$10^{10}$	.968 (.070)	.949 (.087)	.969 (.070)	.965 (.097)	.974 (.062)	.967 (.069)	.968 (.068)	.950 (.086)	.963 (.083)
300	50	$10^5$	.948 (.107)	.961 (.077)	.960 (.073)	.962 (.092)	.945 (.110)	.945 (.106)	.962 (.082)	.961 (.073)	.960 (.081)
		$10^{10}$	.948 (.107)	.961 (.077)	.960 (.073)	.962 (.092)	.945 (.110)	.945 (.106)	.962 (.082)	.961 (.073)	.960 (.081)
500	50	$10^5$	.967 (.070)	.956 (.079)	.971 (.064)	.954 (.102)	.955 (.093)	.963 (.078)	.959 (.080)	.953 (.088)	.969 (.059)
		$10^5$	.967 (.070)	.956 (.079)	.971 (.064)	.954 (.102)	.955 (.093)	.963 (.078)	.959 (.080)	.953 (.088)	.969 (.059)

Table A.1: Mean (*standard deviation*) coverage of 95% credible intervals for band-collapsed measures from 100 random samples of  $N$  conditional MA(2) time series of length  $n$  using hyperparameter  $G$ .

1999). We defined the integrated square error (ISE) of an estimate  $\hat{f}_p^{HF}$  of  $f_p^{HF}$  as

$$\int_0^1 \left[ \hat{f}_p^{HF}(u) - f_p^{HF}(u) \right]^2 du.$$

The ISEs for  $\hat{f}_p^{LF/HF}$  and  $\hat{\rho}_{pq}^{2,HF}$  were similarly defined. The mean and standard deviation of the ISEs are presented in Table A.2. As expected, the ISE of each estimator improved with an increase in either  $n$  or  $N$ . The insensitivity of the proposed procedure to choice of hyperparameter that was observed through indistinguishable coverage probabilities was also observed in the ISE; the ISE under  $G = 10^5$  and  $G = 10^{10}$  were identical up to at least three significant digits. In each setting, the proposed estimator had smaller mean ISE compared to the two-stage procedures.



$n$	$N$	Estimator	$f_1^{HF}$	$f_2^{HF}$	$f_3^{HF}$	$f_1^{LF/HF}$	$f_2^{LF/HF}$	$f_3^{LF/HF}$
300	25	Bayes: $10^5$	6.76 (4.96)	6.75 (6.03)	6.57 (6.30)	2.98 (2.23)	3.28 (2.45)	4.31 (3.34)
		Bayes: $10^{10}$	6.76 (4.96)	6.75 (6.03)	6.57 (6.30)	2.98 (2.23)	3.28 (2.45)	4.31 (3.34)
		2-Stage: Spline	12.11 (12.70)	13.14 (18.56)	12.82 (12.20)	8.75 (8.29)	10.06 (8.29)	8.92 (7.00)
		2-Stage: LOESS	10.31 (6.97)	11.25 (14.06)	11.68 (7.89)	10.01 (7.36)	10.86 (7.36)	10.18 (7.97)
500	25	Bayes: $10^5$	3.75 (2.94)	4.57 (3.54)	3.75 (2.82)	1.86 (1.68)	1.79 (1.29)	2.62 (1.89)
		Bayes: $10^{10}$	3.75 (2.94)	4.57 (3.54)	3.75 (2.82)	1.86 (1.68)	1.79 (1.29)	2.62 (1.89)
		2-Stage: Spline	7.87 (7.76)	8.05 (8.63)	7.15 (7.27)	5.26 (4.35)	5.04 (4.80)	4.60 (3.44)
		2-Stage: LOESS	7.93 (6.32)	7.69 (5.29)	7.21 (5.61)	5.94 (3.84)	5.34 (3.50)	5.42 (2.87)
300	50	Bayes: $10^5$	3.33 (2.69)	3.61 (2.84)	3.59 (2.97)	1.51 (1.37)	1.83 (1.39)	2.51 (1.81)
		Bayes: $10^{10}$	3.33 (2.69)	3.61 (2.84)	3.59 (2.97)	1.51 (1.37)	1.83 (1.39)	2.51 (1.81)
		2-Stage: Spline	6.64 (7.70)	7.09 (10.34)	6.84 (6.63)	4.88 (4.15)	5.39 (4.41)	5.57 (4.35)
		2-Stage: LOESS	5.50 (4.00)	5.60 (6.35)	5.91 (4.21)	5.31 (3.64)	5.62 (3.48)	5.79 (3.85)
500	50	Bayes: $10^5$	1.74 (1.25)	2.12 (1.50)	2.06 (1.36)	1.00 (0.83)	1.13 (1.13)	1.44 (0.92)
		Bayes: $10^{10}$	1.74 (1.25)	2.12 (1.50)	2.06 (1.36)	1.00 (0.83)	1.13 (1.13)	1.44 (0.92)
		2-Stage: Spline	4.52 (5.00)	4.87 (5.31)	3.84 (4.31)	2.87 (2.56)	3.19 (3.07)	2.84 (2.32)
		2-Stage: LOESS	3.85 (3.13)	3.89 (2.89)	3.47 (2.41)	2.81 (1.92)	3.04 (2.18)	2.79 (1.57)

Table A.2: Mean (*standard deviation*) of the integrated square error (ISE) of band-collapsed measures from 100 random samples of  $N$  independent conditional MA(2) time series of length  $n$ . Estimates were obtained using the proposed procedure with tuning parameter  $G = 10^5$  (Bayes:  $10^5$ ) and  $G = 10^{10}$  (Bayes:  $10^{10}$ ) and two-stage estimators using smoothing splines (2-Stage: Spline) and local linear regression (2-Stage: LOESS). Values are reported  $\times 10^3$  for HF measures and  $\times 10^5$  for LF/HF measures.

## B Details of the Sampling Scheme

In this appendix we provide more details about the sampling scheme outlined in Section 4.3, assuming  $P = 3$ . As in Section 4.3,  $\mathbf{q}'_{rjm}$ ,  $\mathbf{q}'_{ijm}$  or  $\mathbf{q}'_{djm}$  are the rows of  $Q_r$ ,  $Q_i$  and  $Q_d$ , respectively, corresponding to  $u_j$  and  $\omega_m$ . The corresponding DFT value is denoted by  $y_{pjm}$ . The elements of  $\Theta(\omega, u)$  in Equation (4.2) are expressed as

$$\theta_{kljm} = \mathbf{q}'_{rjm} \boldsymbol{\eta}_{rkl} + i \mathbf{q}'_{ijm} \boldsymbol{\eta}_{ikl}, \quad k > \ell = 1, \dots, P-1, \quad (\text{B.1})$$

where the  $i$  in the second term on the right-hand side of (B.1) is the unit imaginary number. The diagonal elements of  $\Psi^{-1}(\omega, u)$  are expressed as  $\psi_{kkjm}^{-1} = \exp(\mathbf{q}'_{djm} \boldsymbol{\eta}_{dkk})$ ,  $k = 1, \dots, P$ .

### Drawing the Basis Function Coefficient Vectors

The conditional posterior distribution of  $\boldsymbol{\eta}_{ck\ell}$ ,  $c = r, i$ ,  $k > \ell = 1, \dots, P-1$ , is multivariate normal,  $N(\boldsymbol{\mu}_{ck\ell}, \Sigma_{ck\ell})$ . In what follows we provide expressions for  $\boldsymbol{\mu}_{ck\ell}$  and  $\Sigma_{ck\ell}$ .

*Mean vectors and covariance matrices for  $\boldsymbol{\eta}_{r21}$  and  $\boldsymbol{\eta}_{i21}$*

$$\begin{aligned} \Sigma_{c21}^{-1} &= 2 \sum_{j=1}^N \sum_{m=1}^M \psi_{11jm}^{-1} |Y_{2jm}|^2 \mathbf{q}_{cjm} \mathbf{q}'_{cjm} + D_{c21}^{-1}, \quad c = r, i \\ \Sigma_{r21}^{-1} \boldsymbol{\mu}_{r21} &= 2 \sum_{j=1}^N \sum_{m=1}^M \psi_{11jm}^{-1} \Re \{ Y_{1jm} Y_{2jm}^* - \theta_{31jm}^* Y_{2jm} Y_{3jm}^* \} \mathbf{q}_{rjm} \\ \Sigma_{i21}^{-1} \boldsymbol{\mu}_{i21} &= 2 \sum_{j=1}^N \sum_{m=1}^M \psi_{11jm}^{-1} \Im \{ Y_{1jm} Y_{2jm}^* + \theta_{31jm}^* Y_{2jm} Y_{3jm}^* \} \mathbf{q}_{ijm}. \end{aligned}$$

Note that  $\psi_{11jm}^{-1}$  and  $\theta_{31jm}$  are evaluated at their current values.

Mean vectors and covariance matrices for  $\boldsymbol{\eta}_{r31}$  and  $\boldsymbol{\eta}_{i31}$

$$\begin{aligned}\Sigma_{c31}^{-1} &= 2 \sum_{j=1}^N \sum_{m=1}^M \psi_{11jm}^{-1} |Y_{3jm}|^2 \mathbf{q}_{cjm} \mathbf{q}'_{cjm} + D_{c31}^{-1}, \quad c = r, i \\ \Sigma_{r31}^{-1} \boldsymbol{\mu}_{r31} &= 2 \sum_{j=1}^N \sum_{m=1}^M \psi_{11jm}^{-1} \Re\{Y_{1jm} Y_{3jm}^* - \theta_{21jm}^* Y_{2jm}^* Y_{3jm}\} \mathbf{q}_{rjm} \\ \Sigma_{i31}^{-1} \boldsymbol{\mu}_{i31} &= 2 \sum_{j=1}^N \sum_{m=1}^M \psi_{11jm}^{-1} \Im\{Y_{1jm} Y_{3jm}^* + \theta_{21jm}^* Y_{2jm}^* Y_{3jm}\} \mathbf{q}_{ijm}.\end{aligned}$$

Mean vectors and covariance matrices for  $\boldsymbol{\eta}_{r32}$  and  $\boldsymbol{\eta}_{i32}$

$$\begin{aligned}\Sigma_{c32}^{-1} &= 2 \sum_{j=1}^N \sum_{m=1}^M \psi_{22jm}^{-1} |Y_{3jm}|^2 \mathbf{q}_{cjm} \mathbf{q}'_{cjm} + D_{c32}^{-1}, \quad c = r, i \\ \Sigma_{r32}^{-1} \boldsymbol{\mu}_{r32} &= 2 \sum_{j=1}^N \sum_{m=1}^M \psi_{22jm}^{-1} \Re\{Y_{2jm}^* Y_{3jm}\} \mathbf{q}_{rjm} \\ \Sigma_{i32}^{-1} \boldsymbol{\mu}_{i32} &= 2 \sum_{j=1}^N \sum_{m=1}^M \psi_{22jm}^{-1} \Im\{Y_{2jm} Y_{3jm}^*\} \mathbf{q}_{ijm}.\end{aligned}$$

The basis function coefficient vectors  $\boldsymbol{\eta}_{dkk}$ ,  $k = 1, \dots, P$ , are drawn from  $p(\boldsymbol{\eta}_{dkk} \mid Q_d, \mathbf{v}_k, D_{dkk})$ , given in Section 4.3. The entries  $v_{kjm}$  of  $\mathbf{v}_k$  for  $k = 1, 2, 3$  are as follows.

$$\begin{aligned}v_{1jm} &= |Y_{1jm}|^2 + |\theta_{21jm} Y_{2jm}|^2 + |\theta_{31jm} Y_{3jm}|^2 \\ &\quad - 2\Re\{\theta_{21jm} Y_{1jm}^* Y_{2jm} + \theta_{31jm} Y_{1jm}^* Y_{3jm} - \theta_{21jm}^* \theta_{31jm} Y_{2jm}^* Y_{3jm}\}. \\ v_{2jm} &= |Y_{2jm}|^2 + |\theta_{32jm} Y_{3jm}|^2 - 2\Re\{\theta_{32jm} Y_{2jm}^* Y_{3jm}\}. \\ v_{3jm} &= |Y_{3jm}|^2.\end{aligned}$$

The vectors  $\boldsymbol{\eta}_{dkk}$ ,  $k = 1, \dots, P$ , are generated independently via a Metropolis-Hastings step with a multivariate  $t$  proposal distribution,  $t_\nu(\hat{\boldsymbol{\eta}}_{dkk}, \hat{\Sigma}_{dkk})$ , where

$$\hat{\boldsymbol{\eta}}_{dkk} = \arg \max_{\boldsymbol{\eta}_{dkk}} \log p(\boldsymbol{\eta}_{dkk} \mid Q_d, \mathbf{v}_k, D_{dkk})$$

and

$$\hat{\Sigma}_{dkk} = \left[ -\frac{\partial^2}{\partial \boldsymbol{\eta}_{dkk} \partial \boldsymbol{\eta}'_{dkk}} \log p(\boldsymbol{\eta}_{dkk} \mid Q_d, \mathbf{v}_k, D_{dkk}) \right]_{\boldsymbol{\eta}_{dkk} = \hat{\boldsymbol{\eta}}_{dkk}}^{-1}.$$

The gradient and Hessian of  $\log p(\boldsymbol{\eta}_{dkk} \mid Q_d, \mathbf{v}_k, D_{dkk})$  are given by

$$\sum_{j=1}^N \sum_{m=1}^M \left[ 1 - v_{kjm} \exp(\mathbf{q}'_{djm} \boldsymbol{\eta}_{dkk}) \right] \mathbf{q}_{djm} - D_{dkk}^{-1} \boldsymbol{\eta}_{dkk}$$

and

$$- \sum_{j=1}^N \sum_{m=1}^M v_{kjm} \exp(\mathbf{q}'_{djm} \boldsymbol{\eta}_{dkk}) \mathbf{q}_{djm} \mathbf{q}'_{djm} - D_{dkk}^{-1},$$

respectively.

### Drawing the Smoothing Parameters

Details are given below for the smoothing parameters associated with the real part of  $\theta_{k\ell}(\omega, u)$ . The details for the rest of the smoothing parameters are similar. The smoothing parameters  $\tau_{\beta rkl}^2$ ,  $\tau_{\gamma rkl}^2$  and  $\tau_{\delta rkl}^2$  are drawn independently for  $k > \ell = 1, \dots, P-1$ , as follows.

$$\begin{aligned} \tau_{\beta rkl}^2 &\stackrel{\text{ind}}{\sim} IG((n_b + \nu)/2, \mathbf{b}'_{rkl} \mathbf{b}_{rkl}/2 + \nu/g_{\beta rkl}) \\ \tau_{\gamma rkl}^2 &\stackrel{\text{ind}}{\sim} IG((n_c + \nu)/2, \mathbf{c}'_{rkl} \mathbf{c}_{rkl}/2 + \nu/g_{\gamma rkl}) \\ \tau_{\delta rkl}^2 &\stackrel{\text{ind}}{\sim} IG((n_d + \nu)/2, \mathbf{d}'_{rkl} \mathbf{d}_{rkl}/2 + \nu/g_{\delta rkl}), \end{aligned}$$

where

$$\begin{aligned} g_{\beta rkl} &\stackrel{\text{ind}}{\sim} IG((\nu + 1)/2, \nu/\tau_{\beta rkl}^2 + 1/G^2) \\ g_{\gamma rkl} &\stackrel{\text{ind}}{\sim} IG((\nu + 1)/2, \nu/\tau_{\gamma rkl}^2 + 1/G^2) \\ g_{\delta rkl} &\stackrel{\text{ind}}{\sim} IG((\nu + 1)/2, \nu/\tau_{\delta rkl}^2 + 1/G^2). \end{aligned}$$